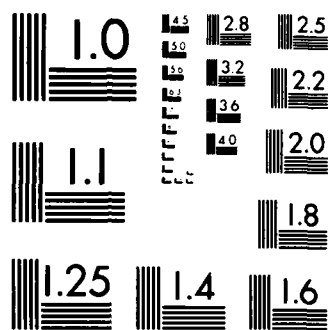END

FILMED

DTIC

MICROCOPY RESOLUTION TEST CHART

NATIONAL BUREAU OF STANDARDS 1963 A

$$\Delta E = \left[\zeta PG/4\pi\lambda^2\right]^{1/2} \frac{a_k(\vec{n}_k \cdot \vec{r}_k)\, g_k f_k e^{-j[2\pi(r_k+R_k)/\lambda + \pi/2]}}{r_k R_k} \tag{6}$$

The field scattered by the reflector is the sum of the elemental field contributed by each patch, taking into account the polarization of each contributor. The polarization of the field radiated by a patch is determined by the incident ray polarization and its transformation on reflection which is given by (Ref. 3):

$$\vec{E} = (\vec{n} \cdot \vec{E}_i)\,\vec{n}_i - (\vec{n}_i \times \vec{E}_i) \times \vec{n}_i \tag{7}$$

# MASSACHUSETTS INSTITUTE OF TECHNOLOGY
## LINCOLN LABORATORY

# ELECTROMAGNETIC SCATTERING BY ARBITRARILY
# SHAPED REFLECTORS: SUBREFLECTOR EFFICIENCY

*A.R. DION*
*L.V. MURESAN*

*Group 61*

TECHNICAL REPORT 662

31 OCTOBER 1984

DTIC
ELECTE
JAN 1 1 1985
S
D
B

**LEXINGTON**                                      **MASSACHUSETTS**

ABSTRACT

A general expression for the electromagnetic scattering by an arbitrary shaped reflector is developed and applied in a computer model of offset hyperboloid reflectors. The computed scattering is shown to be in excellent agreement with scattering measurements made on an offset reflector of projected diameter = 24 cm, at frequencies of 10.35 GHz, 20.7 GHz and 44.5 GHz. Next, using the computer model, the efficiency of the subreflector in a dual-reflector antenna is calculated as a function of subreflector diameter and for two values of illumination taper. For subreflectors truncated at the ray-optics boundary the calculated efficiency is 0.83 and 0.91, respectively, for truncation diameter of 7.7 $\lambda$ and 30.4 $\lambda$, with 5 dB of illumination taper; these respective efficiencies increase to 0.91 and 0.95 with 12 dB of illumination taper. However, subreflectors of diameter about two wavelengths larger than the ray-optics diameter have very nearly unit efficiency.

iii

# CONTENTS

ILLUSTRATIONS

## 1.0 INTRODUCTION

Offset, dual-reflector antennas are finding increased applications, particularly in satellite communications systems. An example is the casse-grain, EHF, multiple-beam antenna depicted in Fig. 1, which consists of an offset paraboloid reflector, an hyperboloidal subreflector and a 4 x 4 array of feed horns. The beam produced by this antenna is shaped to cover a desired area on the earth from a synchronous altitude satellite.

The subreflector of a dual-reflector antenna is generally made a little larger than the boundary determined by the intersection of the subreflector with the focal cone of rays bounding the reflector (ray-optics boundary). The slightly larger size is required to compensate for the effects of edge dif-fraction, which would reduce antenna gain if the subreflector was truncated at the ray-optics boundary. On the other hand, making the subreflector much lar-ger than the ray-optics boundary is generally detrimental due to either increased blockage of secondary radiation or increased weight and size. The determination of the minimum size of the subreflector in a dual-reflector antenna is a subject treated in this report. It will be shown, in particular, that truncation of the subreflector at the ray-optics boundary causes appre-ciable loss of antenna gain, due to subreflector edge diffraction, but trun-cation at least one wavelength beyond this boundary renders the loss negli-gible. This result was obtained by physical-optics analysis, using a computer modelling technique which was also used in a related study of scattering by
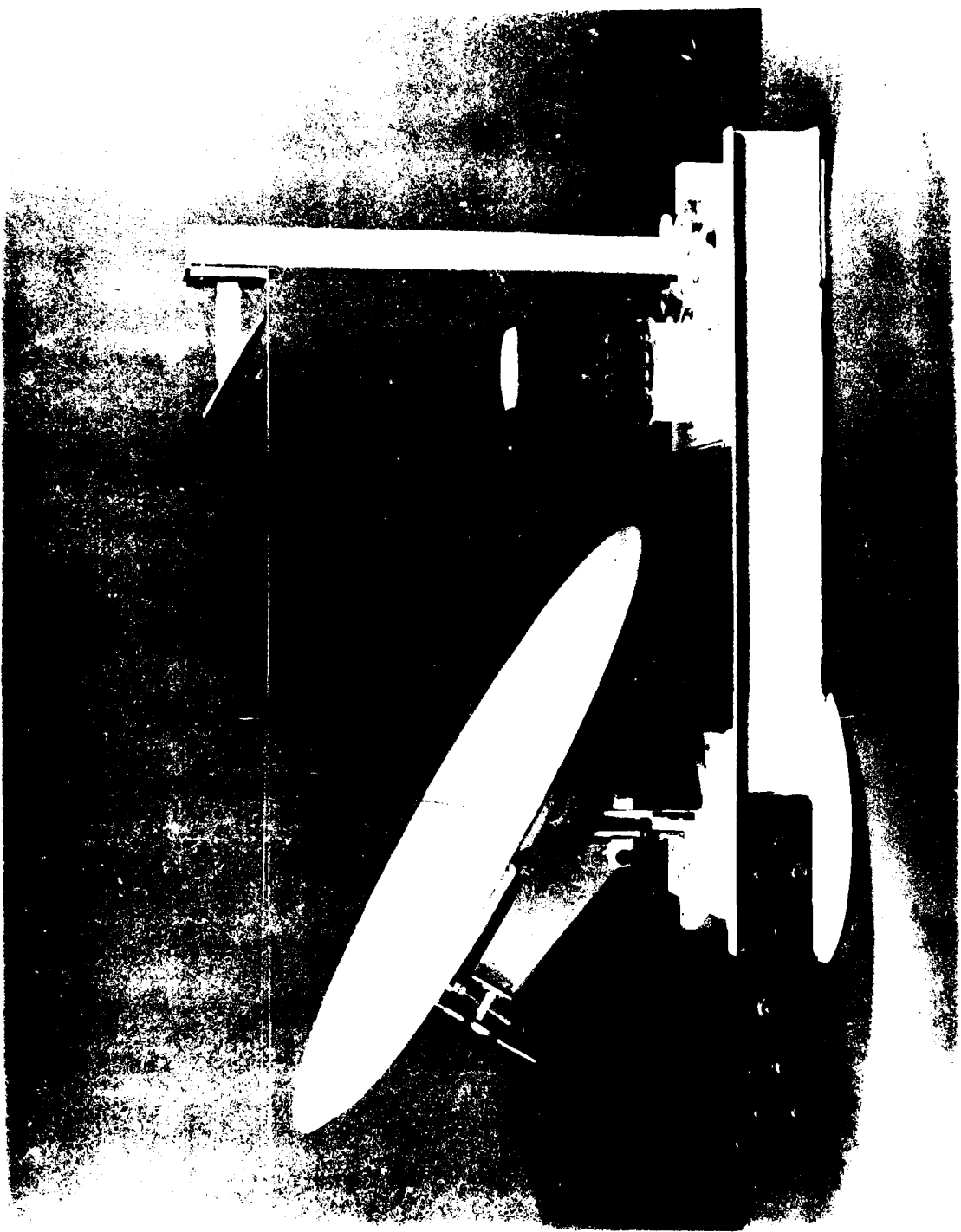
Fig. 1.  EHF multiple beam antenna.

CR-202-3363

offset hyperboloidal reflectors. The latter study, which was complemented by
an experimental verification in excellent agreement with the computer model,
and a similar study based on ray-optics analysis are also presented here.

In this report, a general expression of the field produced by an arbi-
trary reflector and feed is developed and applied in a computer model of off-
set hyperboloidal reflectors. This expression is an extension of a formula-
tion developed several years ago to determine the effects of surface devia-
tions on the radiation patterns of large reflectors (Ref. 1). In recent years
this expression has been very useful in developing computer models of multi-
ple-beam antennas of various configurations, particularly, offset, single- and
dual-reflector antennas and lens antennas (Ref. 2). These models proved to be
very effective, requiring short computer execution times and providing accu-
rate performance data. An important feature of the modelling technique is
that it applies equally well to symmetric or asymmetric configurations, to
focused or defocused systems, to far-field or near-field characteristics.
Although a large core memory is generally required, the execution time is
short, being about 0.01 second per observation point, using a computer capable
of 10.5 million instructions per second. This value of execution time applies
to collimating reflectors with conventional point-source illuminations and
provides for radiation patterns with an error that increases quadratically
from negligible to about 1 dB at the fifth sidelobe from broadside. For non-
collimating reflectors execution time increases and is a function of reflector

size in wavelengths. For the largest subreflector included in this study the
execution time was ≈0.1 second per observation point.

The computer model of offset hyperboloidal reflectors was validated by
scattering measurements made on the subreflector of the antenna shown in
Fig. 1. Corrugated, conical horns were used to illuminate the offset
reflector with a taper of about 5 dB, at frequencies of 44.5 GHz, 20.7 GHz and
10.35 GHz, corresponding to projected diameter-to-wavelength ratios of about
35.6, 16.6 and 8.3, respectively.

## 2.0 ANALYSIS

### 2.1 Basic Formulation for Computer Modelling

Let the arbitrary shaped reflector of Fig. 2a be illuminated by a feed with input power P and directivity G, and let its surface be divided into N patches of approximately equal area, $a_k$, and of dimensions small enough so that over the extent of a patch the incident field is essentially uniform. The power, $P_k$, intercepted by the $k^{th}$ patch is then:

$$P_k = \frac{PG \, |g_k|^2 \, a_k(\vec{n}_k \cdot \vec{r}_k)}{4\pi \, r_k^2} \qquad (1)$$

where $G|g_k|^2$ is the feed directive gain in the directic    the patch,

$a_k(\vec{n}_k \cdot \vec{r}_k)$ is the area of the patch projected in a plane normal to the direction of incidence,

$\vec{n}_k$ is the unit vector normal to the patch at its center

$\vec{r}_k$ is the unit vector specifying the incident ray direction,

$r_k$ is the distance between the feed and the patch centers.

At the center of the patch, the phase of the incident field is delayed with respect to the field at the feed aperture by

$$\phi_k^i = 2\pi \, r_k/\lambda \qquad (2)$$

Consider next the reflected wave at a patch and assume it to be plane in the vicinity of the patch. This assumption is valid for collimating reflectors, whatever the patch size. For non-collimating reflectors the condition of a reflected plane wave is an approximation whose accuracy increases with decreasing patch size. In the vicinity of a patch, the reflected field can be considered to be the segment $a'_k$ of a plane wave, as illustrated in
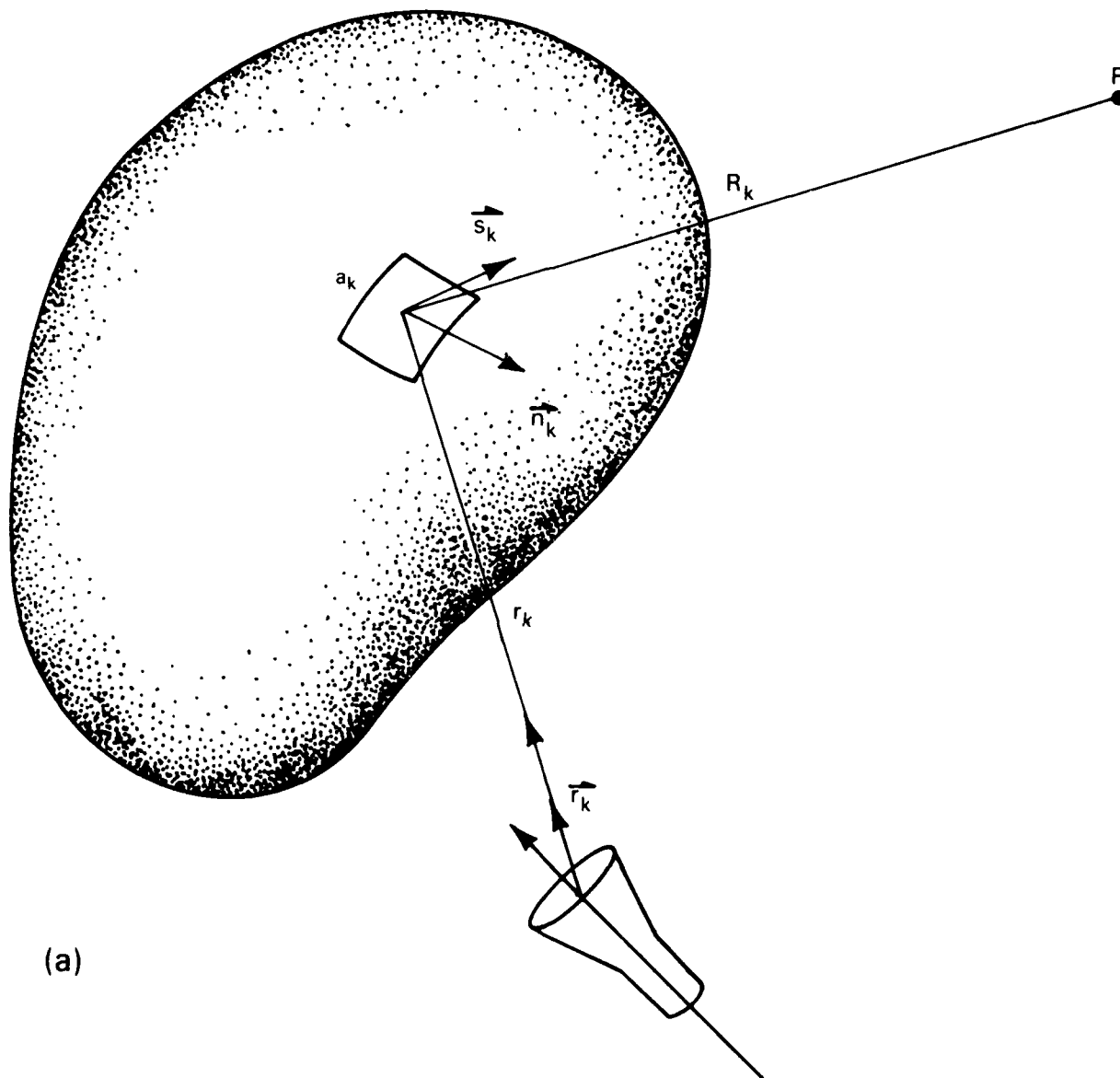
(a)

Fig. 2a.  Arbitrary reflector and feed illustrating typical patch.

6

Fig. 2b, where $\vec{s}_k$ is the unit vector specifying the reflected ray direction. This segment may be treated as a secondary radiator which, at a far-field distance $R_k$, gives rise to an elemental field, $\Delta E$, of power density

$$|\Delta E|^2/\zeta = P_k D_k |f_k|^2 / 4\pi R_k^2 \tag{3}$$

where $\zeta$ is the intrinsic impedance of free space, $|f_k|^2$ is the radiation pattern of a fictitious radiator replacing segment $a_k'$, and $D_k$ is its directivity given by

$$D_k = 4\pi a_k(\vec{n}_k \cdot \vec{r}_k)/\lambda^2 \tag{4}$$

where $a_k(\vec{n}_k \cdot \vec{r}_k) = a_k(\vec{n}_k \cdot \vec{s}_k) = a_k'$ is the area of the patch projected in the plane normal to the reflected ray. The field of this fictitious radiator has a phase which is delayed with respect to the field incident on a patch by:

$$\phi_k^r = 2\pi R_k/\lambda + \pi/2 \tag{5}$$

(The fixed $\pi/2$ delay reflects the quadrature relationship between field and source and is included to provide the complete phase of the field, for later comparison with the ray-optics solution.)

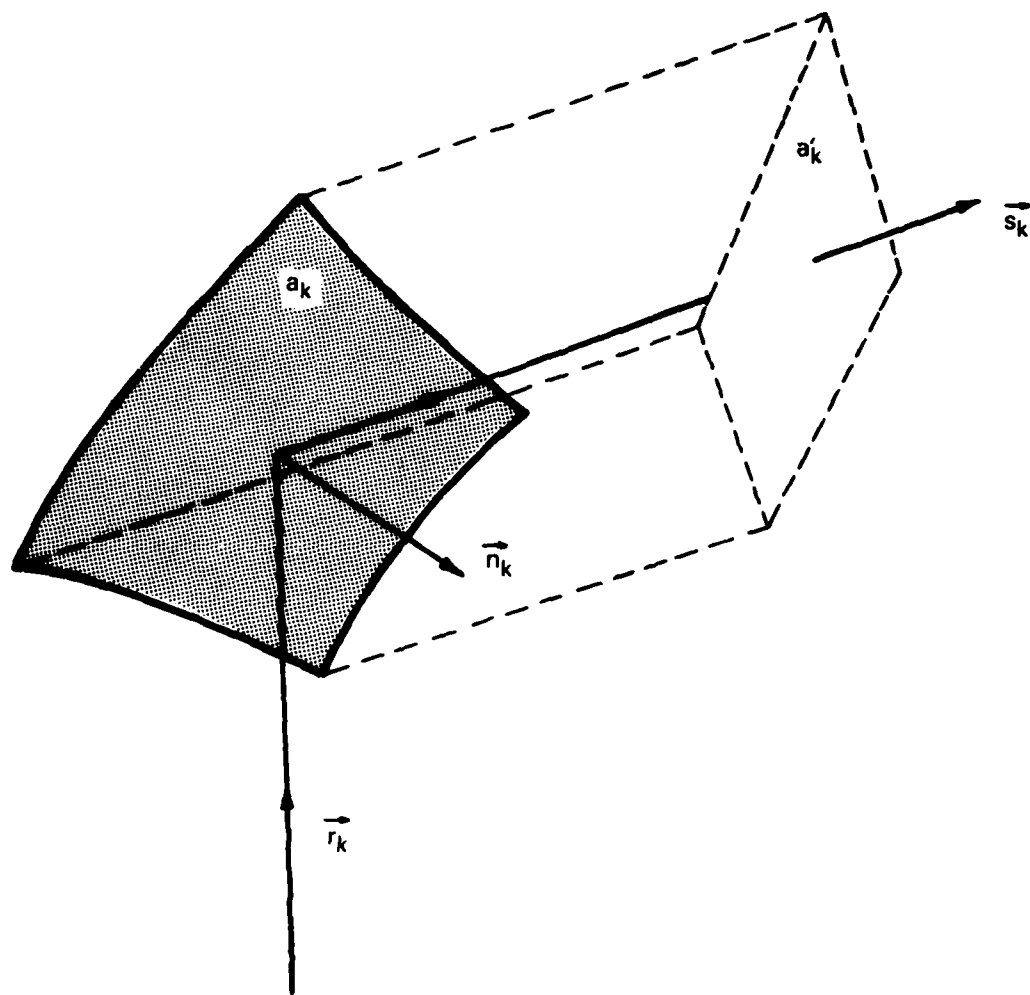Substituting Eqs. (1) and (4) in (3) and expressing the field in complex form yields:

Fig. 2b. Reflected wavefront near a patch.

$$\Delta E = \left[\zeta PG/4\pi\lambda^2\right]^{1/2} \frac{a_k(\vec{n}_k \cdot \vec{r}_k)\, g_k f_k e^{-j[2\pi(r_k+R_k)/\lambda + \pi/2]}}{r_k R_k} \tag{6}$$

The field scattered by the reflector is the sum of the elemental field contributed by each patch, taking into account the polarization of each contributor. The polarization of the field radiated by a patch is determined by the incident ray polarization and its transformation on reflection which is given by (Ref. 3):

$$\vec{E}_r = (\vec{n}_k \cdot \vec{E}_i)\, \vec{n}_k - (\vec{n}_k \times \vec{E}_i) \times \vec{n}_k \tag{7}$$

where $\vec{E}_r$ and $\vec{E}_i$ are, respectively, the reflected and incident field on a patch. The field radiated by a patch has complex amplitude given by Eq. (6) and polarization given by Eq. (7) and must be resolved into three orthogonal components for summation. However, as the point of observation recedes from the reflector, all contributions become polarized in the plane transverse to the direction of propagation, leaving two components of polarization to be summed. In the application that follows the reflected field is considered polarized in the same direction everywhere and, therefore, the far field at distance R is (see Fig. 3):
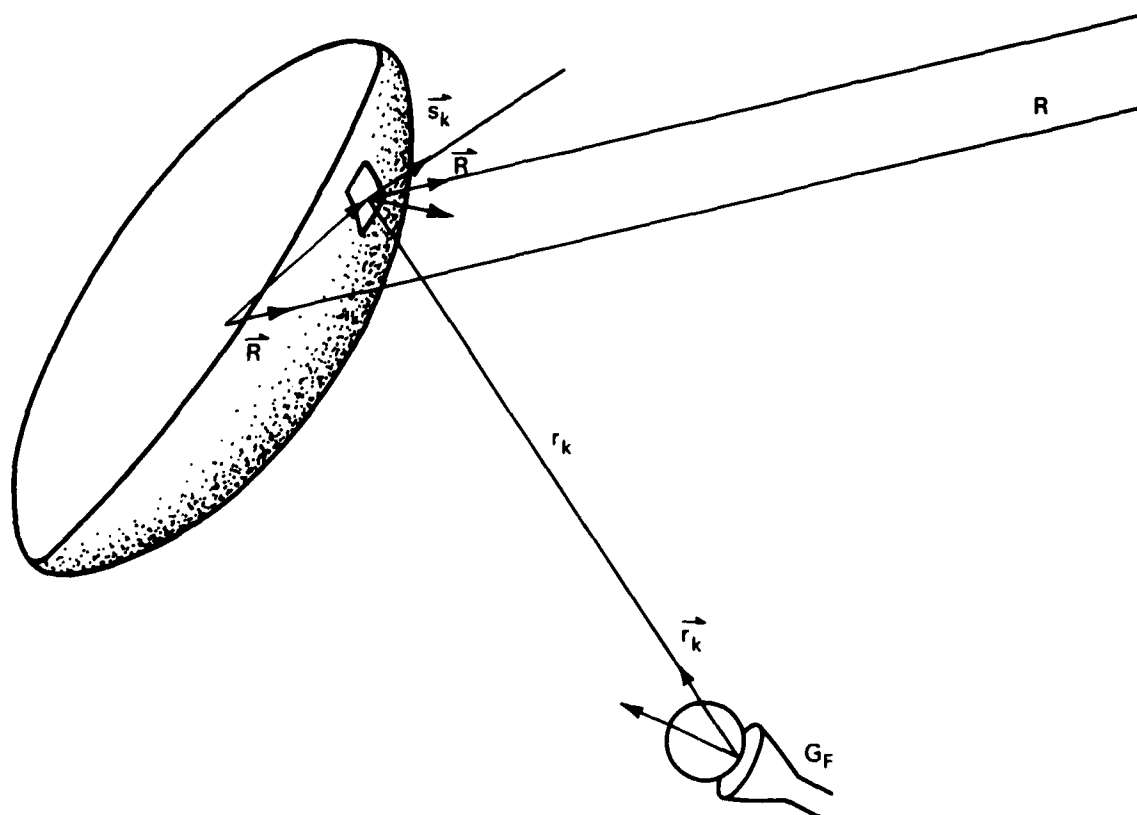
$$E = F[PG\zeta/4\pi R^2\lambda^2]^{1/2} \tag{8}$$

where

-9-

Fig. 3. Geometry for far-field analysis.

10

$$F = \sum_{k=1}^{N} \frac{a_k(\vec{n}_k \cdot \vec{r}_k) \, g_k f_k e^{-j[2\pi(r_k - \vec{\rho}_k \cdot \hat{R})/\lambda + \pi/2]}}{r_k} \tag{9}$$

and $\vec{\rho}_k$ is the patch position vector and $\hat{R}$ is the unit direction vector. The corresponding power density is

$$P_D = |E|^2/\zeta = PG|F|^2/4\pi R^2 \lambda^2 , \tag{10}$$

which normalized to the isotropic power ($=P/4\pi R^2$) yields the directive gain:

$$D = \frac{G}{\lambda^2} \left| \sum_{k=1}^{N} \frac{a_k(\vec{n}_k \cdot \vec{r}_k) \, g_k f_k e^{-j[2\pi(r_k - \vec{\rho}_k \cdot \hat{R})/\lambda]}}{r_k} \right|^2 \tag{11}$$

Equation (11) expresses the field characteristics in a form convenient for computer solution. It should be noted that the formulation is general and, therefore, applies to any surface or any illumination meeting the conditions of its derivation. When applied to a particular case, a convenient system of coordinates is defined and the various parameters in Eq. (11) are expressed in that system. All variables in Eq. (11) are known or readily computed, except for $f_k$ which is the patch radiation pattern. The treatment of this variable depends on the reflector type and on the desired field characteristics. In cases where the field is collimated into a beam, and the field characteristics are required only in the near sidelobe region, it is only necessary to make the patches small enough so that their radiation pattern is uniform in the region of interest, i.e., $f_k = 1$. In cases where the field

produced by the reflector is divergent and the field characteristics are
desired over a wide angular region, the patch size must be made smaller and an
appropriate expression for $f_k$ must be used. One such case is the applica-
tion that follows where it was found necessary to make the patch size slightly
smaller than one wavelength, and where the patch radiation pattern was taken
equal to $\cos \theta$, where $\theta$ is the angle measured from the reflected ray direc-
tion. In this application the patches essentially reduce to Huygens sources.

The number of patches, N, must be chosen so that the conditions of a
plane reflected wave in the vicinity of the patches, and of uniform amplitude
illumination over a patch are satisfied, as well as the condition previously
stated for the choice of $f_k$. The number of patches required is best deter-
mined by tests where N is increased until convergence is reached within a spe-
cified error. For the practical case of the collimating reflector with con-
ventional illumination taper, and modelled with isotropically radiating
patches ($f_k = 1$), the error increases quadratically with angle from bore

sight and is about 1 dB at an angle equal to $.25 \sqrt{\bar{N}}$ beamwidths.

2.2  Total Field

The total field is the sum of the direct field from the feed and of the
field scattered by the reflector as given by Eq. (8). However, the field that
exists in the shadow region of the reflector is that caused by diffraction
around the reflector. In this region the field was calculated by applying
Babinet's principle (Ref. 4) which allows replacement of the reflector by its
complementary aperture in an infinite screen. The field diffracted by this

aperture may be calculated by integrating over the surface of the reflector, thus allowing Eq. (8) to be used, but with the patch normal reversed and with $f_k = \cos\theta$, where $\theta$ is now measured from the incident ray direction. The aperture diffracted field thus computed is subtracted from the incident field (in absence of the screen) to yield the field in the shadow region, as prescribed by Babinet's principle.

## 2.3  Geometrical Optics Solution for Offset Hyperboloids

In this section, the field reflected by an offset hyperboloid is calculated by application of geometrical optics principles, which state that a pencil of rays issued from a feed at the external focus $F_1$ is reflected as a pencil of rays coming from a virtual feed at the internal focus $F_2$. The relevant geometry is presented in Fig. 4 where the spherical coordinates $\theta$, $\phi$ specify the direction of observation. Let the directive gain of the feed be $D_f(\alpha)$ and that of the virtual feed be $D_s(\beta)$, where the incident ray direction, $\alpha$, and the reflected ray direction, $\beta$, are measured from the hyperboloid axis, then for conservation of energy

$$D_f(\alpha) \sin\alpha \, d\alpha = D_s(\beta) \sin\beta \, d\beta \tag{12}$$

The incident and reflected ray directions are related by

$$\tan(\beta/2) = M\tan(\alpha/2) \tag{13}$$

where $M = (1+e)/(1-e)$ is the magnification factor, and e is the eccentricity of the hyperboloid. Taking the derivative on both sides of Eq. (13) yields,

$$d\alpha/d\beta = \cos^2(\alpha/2)/M\cos^2(\beta/2) \tag{14}$$

which substituted in Eq. (12), and after some manipulation, gives

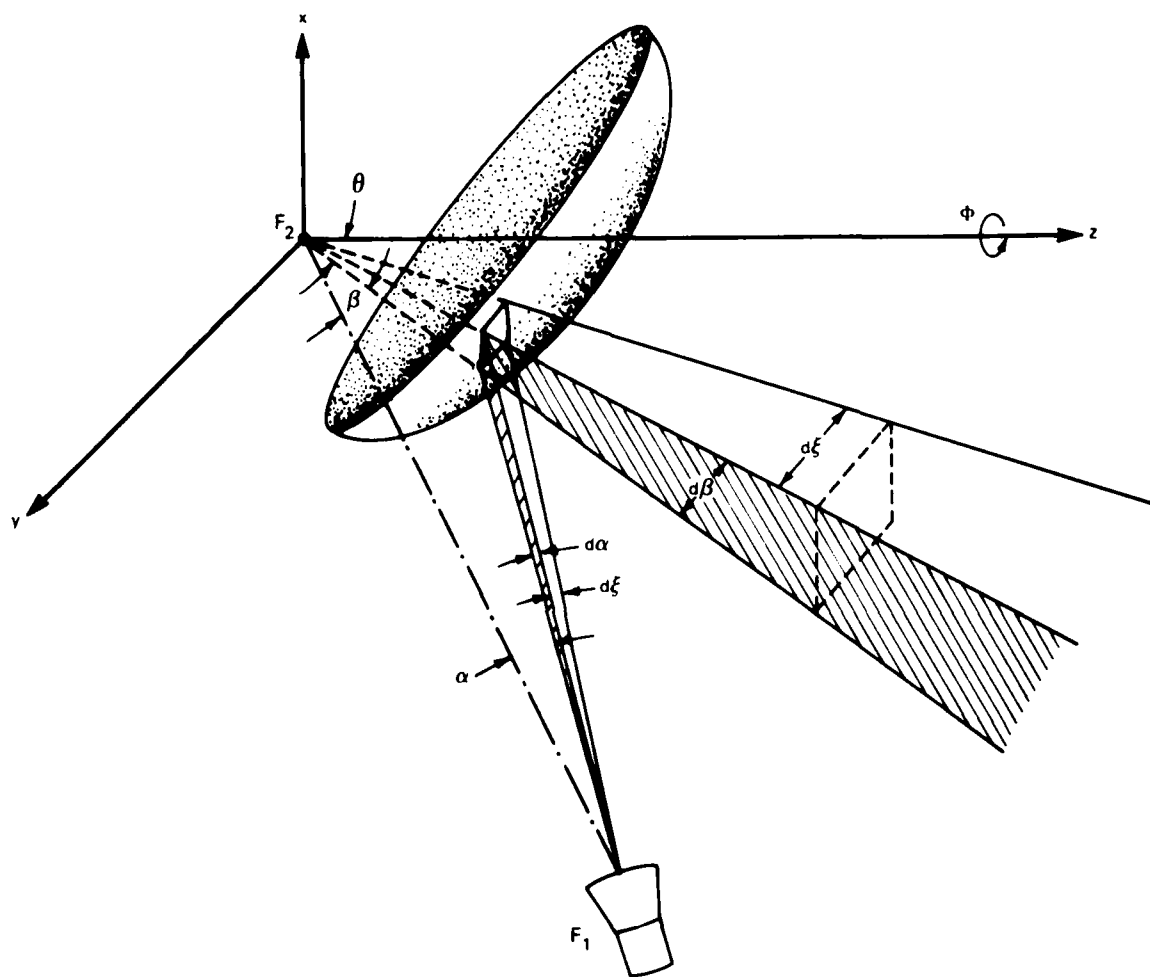$$D_s(\beta) = D_f(\alpha) \cos^4(\alpha/2)/M^2 \cos^4(\beta/2) \tag{15}$$

-13-

Fig. 4.   Incident and reflected pencil of rays on offset hyperboloid.

14

To apply Eq. (15), the direction of the reflected ray, $\beta$, is first computed using

$$\cos \beta = \vec{u} \cdot \vec{v}$$

where the unit vectors $\vec{u}$ and $\vec{v}$ are, respectively, the direction of observation and the direction of the hyperboloid axis, in the $\theta$, $\phi$ coordinate system. The corresponding incident ray direction, $\alpha$, is next computed using Eq. (13), and together with $\beta$ is substituted in Eq. (15) to provide the directive gain of the virtual feed in the direction of observation.

## 2.4 Application to Specific Cases

The general formulation (physical optics) given by Eq. (11) is now applied to the calculation of the field scattered by an offset hyperboloid. For this, the surface of the reflector is specified by N patches whose areas, coordinates and normal at their center must be calculated. For reflectors projecting into a plane as a circle, which is the case here, the patch parameters are obtained by dividing the projected circle into rings of equal width, and further dividing each ring into sectors of width about equal to the ring width, such as illustrated in Fig. 5. Projecting the sectors back onto the hyperboloidal reflector surface then yields the coordinates at the center of each patch where the patch normal and area are determined. The feed illuminating the reflector is modelled by specifying its aperture center, its axis direction, its directivity and its radiation pattern. A rectangular coordinate system with origin at the internal focus of the hyperboloid is chosen to
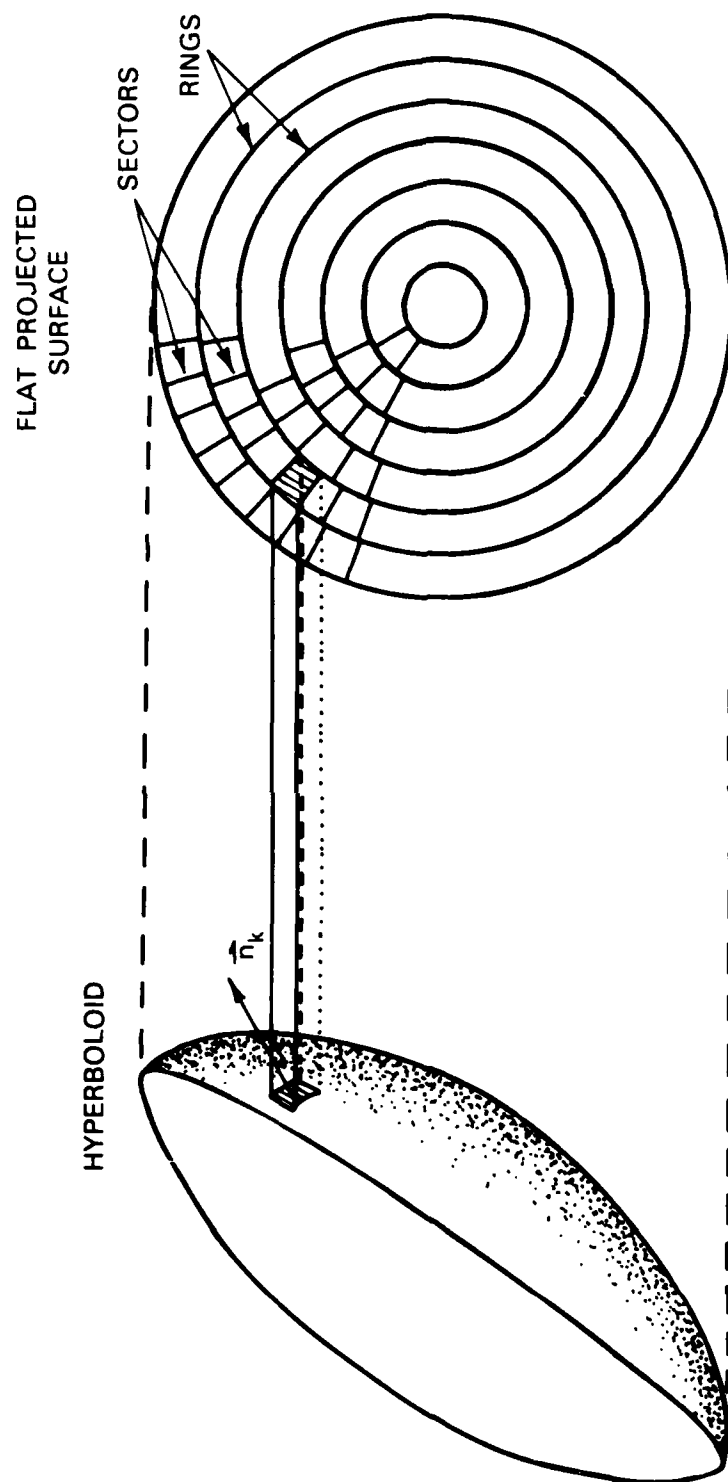
Fig. 5. Patch division for reflector with circular projection.

16

express the geometry of the reflector and feed. The field characteristics are expressed in a spherical coordinate system with origin also at the internal focus of the hyperboloid, and therefore at the phase center (geometrical optics) of the reflected wave. In an initial test of the computer model the results were found in very good agreement with the analytical results of Rusch (Ref. 5) for the uniformly illuminated, centered hyperboloid (a special case of the offset hyperboloid), as indicated by the comparison presented in Fig. 6.
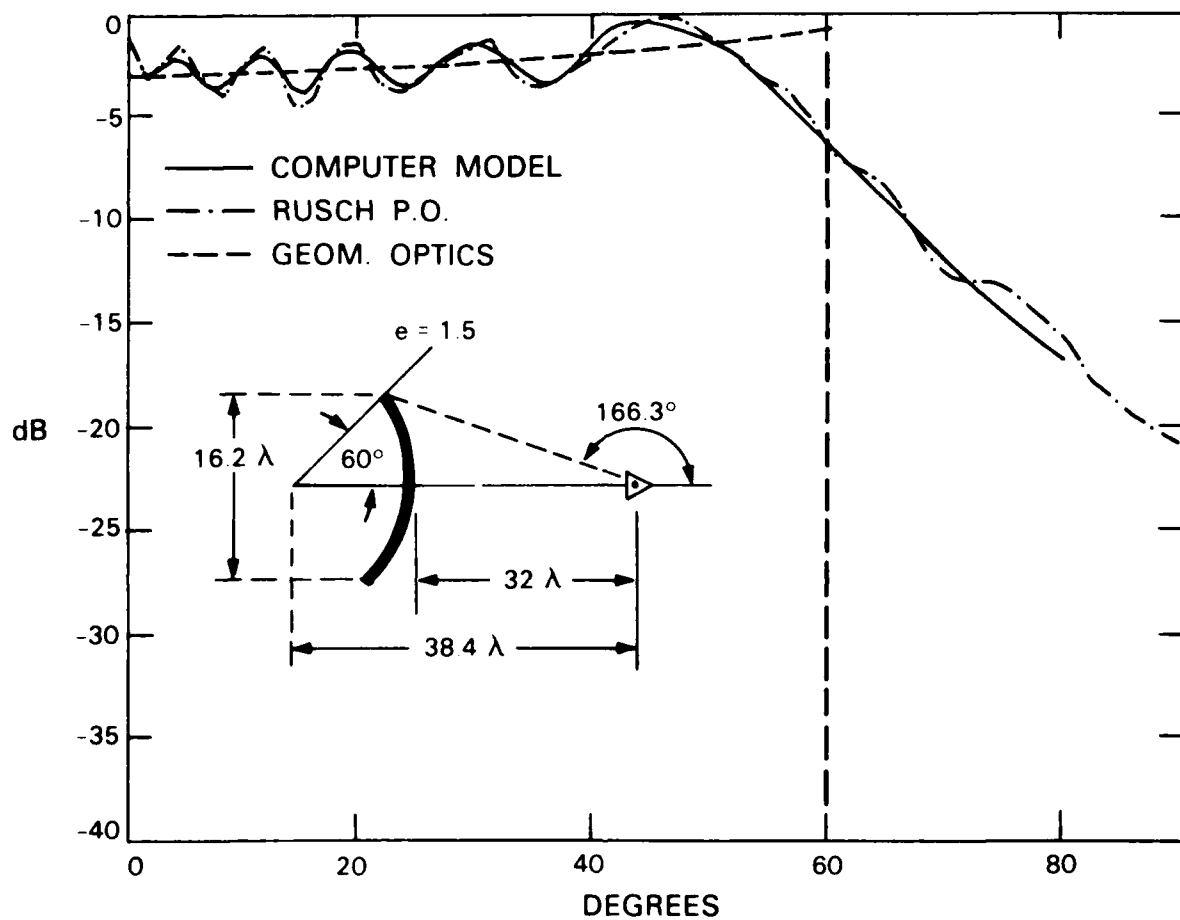
Fig. 6. Scattering by axially symmetric hyperboloid reflector.

## 3.0  EXPERIMENTAL OFFSET HYPERBOLOIDAL REFLECTOR

The offset hyperboloid used in the experimental investigation is the sub-reflector of the offset, dual-reflector antenna presented in Fig. 1. This hyperboloid is characterized by a distance between focii of 52.1 cm and by an eccentricity of 1.715. Its perimeter is the intersection with a cylinder of diameter = 24 cm, whose axis is inclined 17.38° from the hyperboloid axis, as shown in Fig. 7. The feed is located at the external focus of the hyperboloid and its axis, at an angle of 15.25° from the hyperboloid axis, is congruent to the ray which after reflection defines the $\theta = 0°$ direction of the field pattern. Scattering patterns were measured at three frequencies, 44.5 GHz, 20.7 GHz and 10.35 GHz, corresponding to reflector diameters  (circular projection) of 35.6 $\lambda$, 16.56 $\lambda$, and 8.28 $\lambda$, respectively. Measurements were taken in the principal planes $\phi = 0°$ (the plane of offset), and $\phi = 90°$ (the plane of pattern symmetry), and for both parallel and perpendicular polarizations. The feed horn, reflector and mount are shown in Fig. 8. The hyperboloid reflector is mounted on a foam support, and together with the feed horn rotates about an axis passing through the internal focus as defined in Fig. 7. In Fig. 9, the reflector is shown with the alignment template used to ensure correct positioning of the feed at the external focus of the hyperboloid. The feed for each test frequency is a corrugated, conical horn producing a taper of about 5 dB at the edge of the reflector. The measured radiation patterns of the three horns and their aperture dimensions are given in Fig. 10. Also shown in Fig. 10 are the theoretical feedhorn radiation patterns (Ref. 6) used in the scattering calculations, and excellent agreement is observed over the angular sector subtended by the hyperboloid.
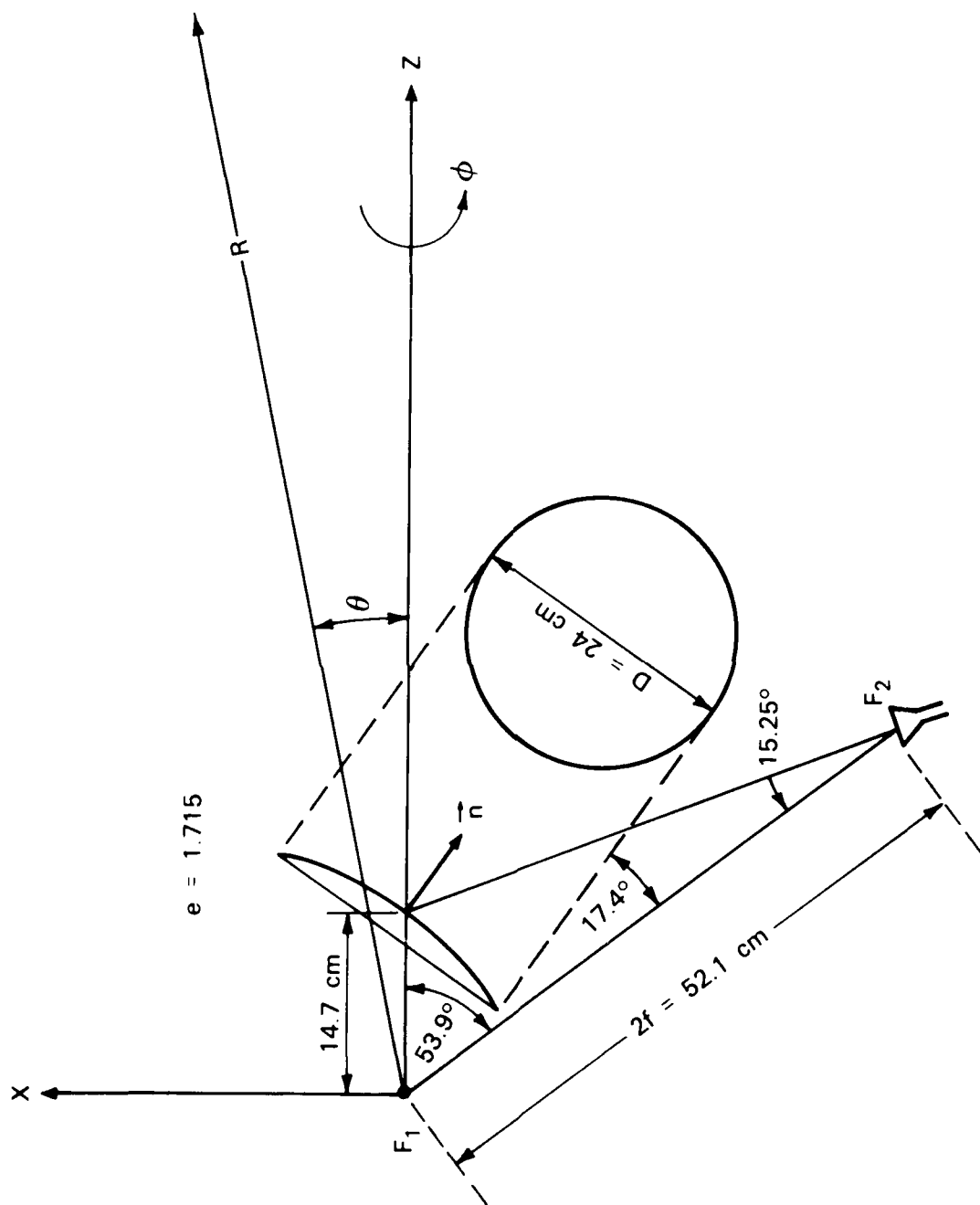
-19-

Fig. 7. Geometry of offset hyperboloidal reflector and field coordinate system.
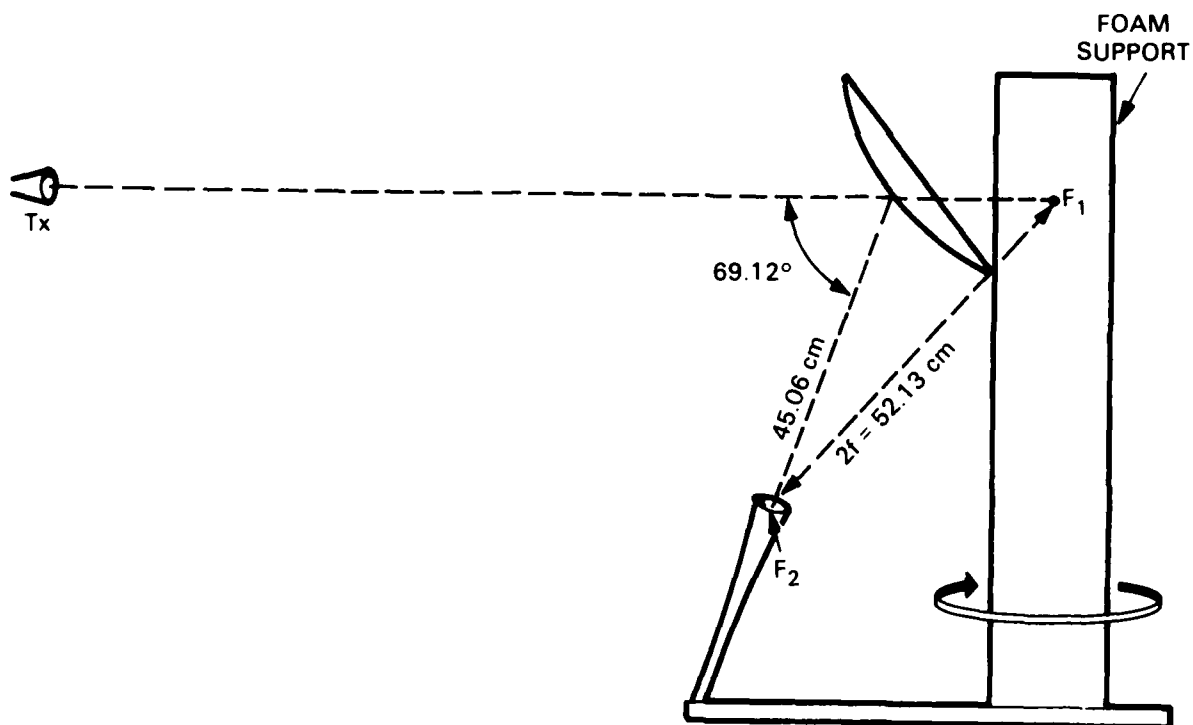
1 30 393-N

Fig. 8. Feed and reflector arrangement for scattering pattern
measurements.

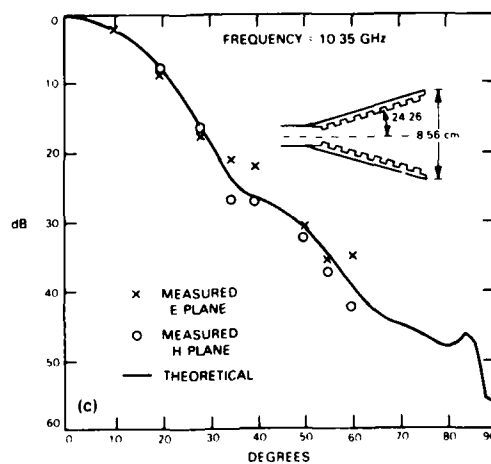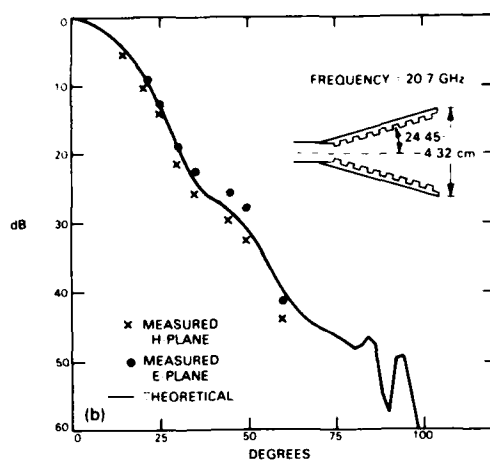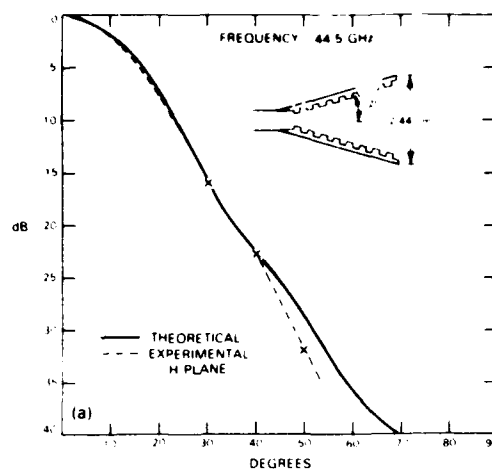Fig. 9. Offset reflector and 10.35-GHz horn with alignment template in place.

1 FOOT

P-185-630

22

Fig. 10. Radiation patterns and aperture dimensions of corrugated feed horns. The half-angle of the 10.35-GHz horn should read 12.2° and not 24.26°.

## 3.1 Results

The principal-plane, calculated and measured (perpendicular polarization) scattering patterns at 44.5 GHz (35.6 $\lambda$ reflector) are shown in Fig. 11. The agreement is good, except at the lower angles in the offset plane, where the effect of feed blockage is substantial. Misalignment, stray reflections, blockage and scattering by the feed and support are believed to account in great part for the differences observed. Geometrical-optics analysis is seen to provide accurately the mean value of the field, except at the reflection region boundary and beyond. At the boundary the intensity of the scattered field is about 6 dB less than predicted by ray optics. The calculated (physical optics) and measured phase patterns are also in excellent agreement. Since the reflector is rotated about its internal focus, i.e., about the apparent center of reflected rays, the geometrical-optics phase pattern is the 0°-phase line. Near the reflection region boundary the phase of the field predicted by geometrical optics is in error by about 30°. The results of scattering measurements made with parallel polarization of the field are nearly identical to those obtained with perpendicular polarization, and are not presented. The measurement region for the 35.6 $\lambda$ reflector included only the reflection region and part of the diffraction region. However, for the 16.6 $\lambda$ and 8.3 $\lambda$ reflectors, the principal-plane patterns all around the reflectors were measured and the results, presented in Figs. 12 and 13, show good agreement with predictions in all regions. The phase patterns, for these two reflectors were measured only over the reflection region, and exhibit somewhat poorer agreement with predictions than for the 35.6 $\lambda$ reflector, but this is likely due to increased blockage by the physically larger feedhorns.
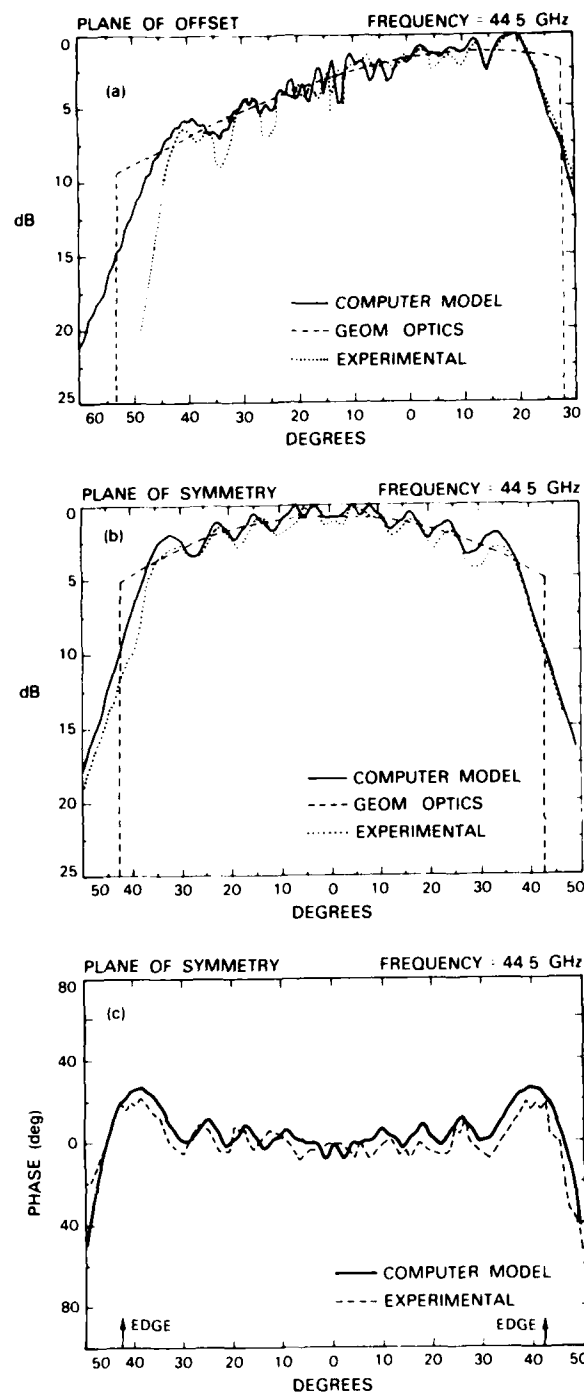
-24-

Fig. 11. Scattering and phase patterns of offset hyperboloidal reflector at 44.5 GHz (projected diameter = 35.6 λ).
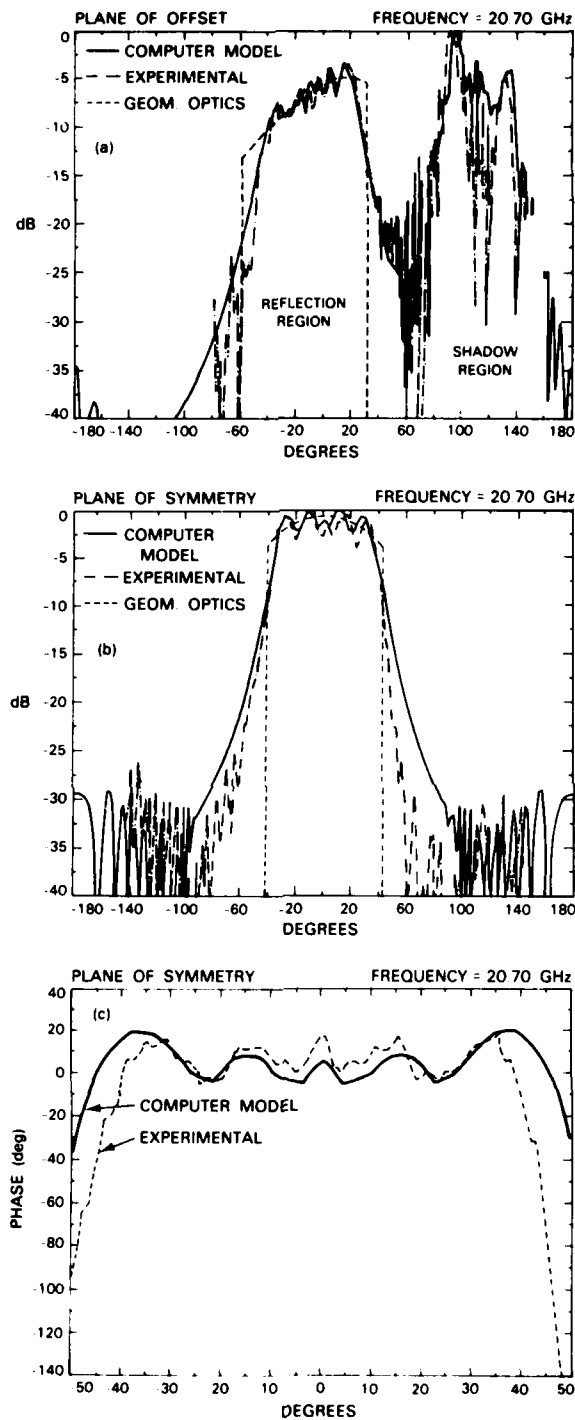
25

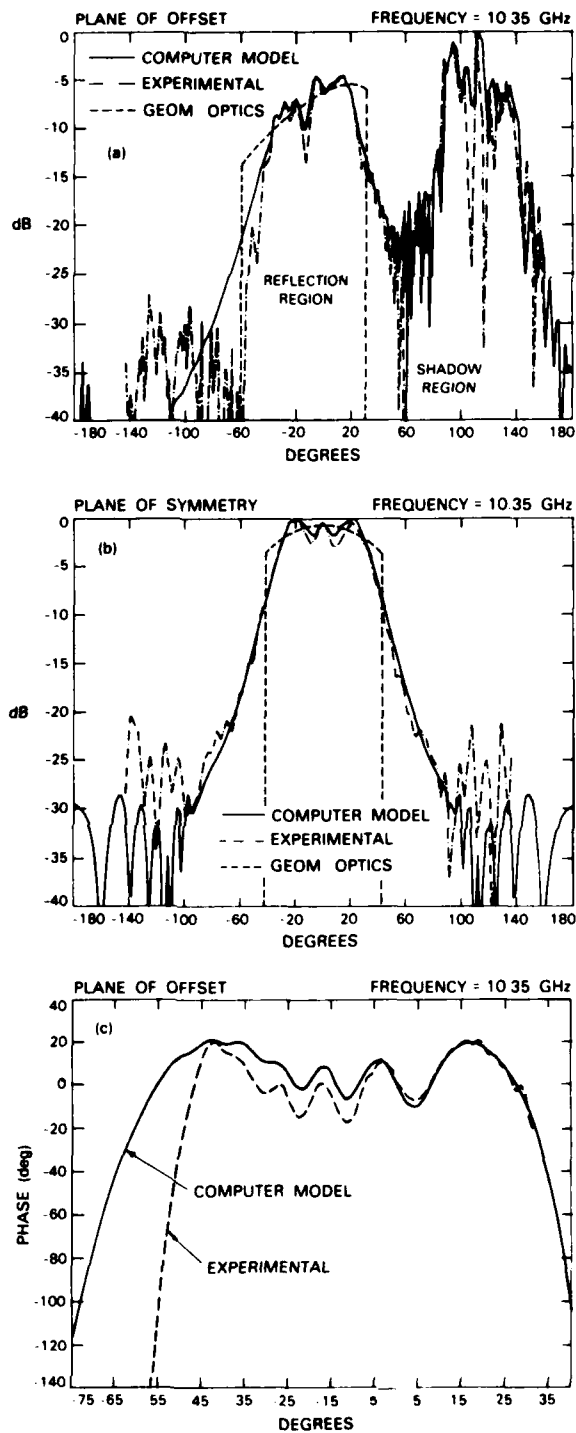Fig. 12. Scattering and phase patterns of offset hyperboloidal reflector at 20.7 GHz (projected diameter = 16.6 λ).

**Fig. 13. Scattering and phase patterns of offset hyperboloidal reflector at 10.35 GHz (projected diameter = 8.3 λ).**

27

## 4.0 EFFECT OF SUBREFLECTOR DIAMETER ON GAIN OF DUAL REFLECTOR ANTENNAS

For reasons of blockage of secondary radiation, or of weight and size, the subreflector of a dual-reflector antenna is, generally, made only as large as is required to optimize performance, and the design guideline has been to truncate the subreflector about one wavelength beyond the ray-optics boundary. In this section, the effect of the subreflector size on the gain of a dual-reflector antenna is calculated, with results that justify the design guideline. The calculations are made for a center-fed, cassegrain antenna, using the computer model previously described. The relevant antenna parameters are given in Fig. 14. The directivity of the dual-reflector antenna is calculated for values of subreflector diameter in the vicinity of the ray-optics value, and does not include blockage effects.

Following Silver (Ref. 7), the directivity of the dual-reflector antenna may be expressed as

$$D_a = \cot^2 (\Psi/2) \left| \int_0^\Psi E(\beta) \tan (\beta/2) \, d\beta \right|^2 \tag{17}$$

where $\Psi$ is the paraboloid half-angle and $E(\beta)$ is the physical-optics solution for the field scattered by the subreflector, which according to Eq. 11, is,

$$E(\beta) = E_{PO}(\beta) = \frac{G}{\lambda}^{1/2} \sum_{k=1}^N \frac{a_k (\vec{n}_k \cdot \vec{r}_k) \, g_k f_k e^{-j2\pi(r_k - \vec{\rho}_k \cdot \hat{R})/\lambda}}{r_k} \tag{18}$$
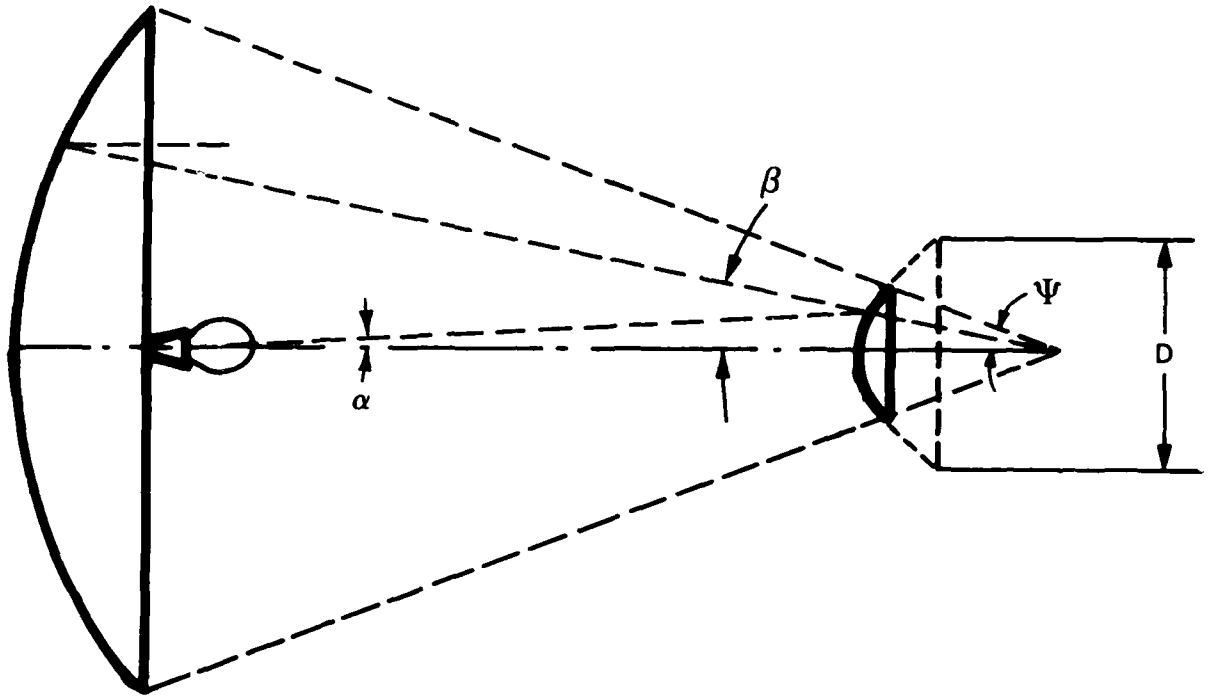
128609-N-01

Fig. 14.  Relevant parameters for subreflector efficiency analysis.

29

The directivity of the dual-reflector antenna is maximum for the subreflector of infinite extent. For this limiting case, the geometrical-optics expression (Eq. (15)) of the scattered field is exact and, the maximum directivity is obtained by substituting it in Eq.(17), i.e.,

$$E(\beta) = E_{GO}(\beta) = D_s^{1/2}(\beta) = \frac{D_f^{1/2}(\alpha)\ \cos^2(\alpha/2)}{M\ \cos^2\ (\beta/2)} \qquad (19)$$

and the maximum directivity is

$$D_a(\max) = \cot^2(\Psi/2)\ \left[\ \int_o^\Psi D_s^{1/2}(\beta)\ \tan\ (\beta/2)\ d\beta\right]^2. \qquad (20)$$

The efficiency of the subreflector of finite size may be expressed as $\eta = D_a/D_a(\max)$, or

$$\eta = \left|\ \int_o^\Psi\ E_{PO}(\beta)\ \tan\ (\beta/2)\ d\beta\ \right|^2 /D_a(\max) \qquad (21)$$

The efficiency of a subreflector is a function of its diameter and of the illumination taper, and was calculated for diameters in the vicinity of ray-optics diameters of 7.7 $\lambda$, 15.5 $\lambda$ and 30.4 $\lambda$, and for tapers at the edge of the reflector of 5 dB and 12 dB. The results are presented in Fig. 15 where the ray-optics truncation diameters (in wavelengths), are indicated by the vertical dotted lines. It is observed that hyperboloid truncation at the ray-optics boundary causes a substantial loss of efficiency, particularly for
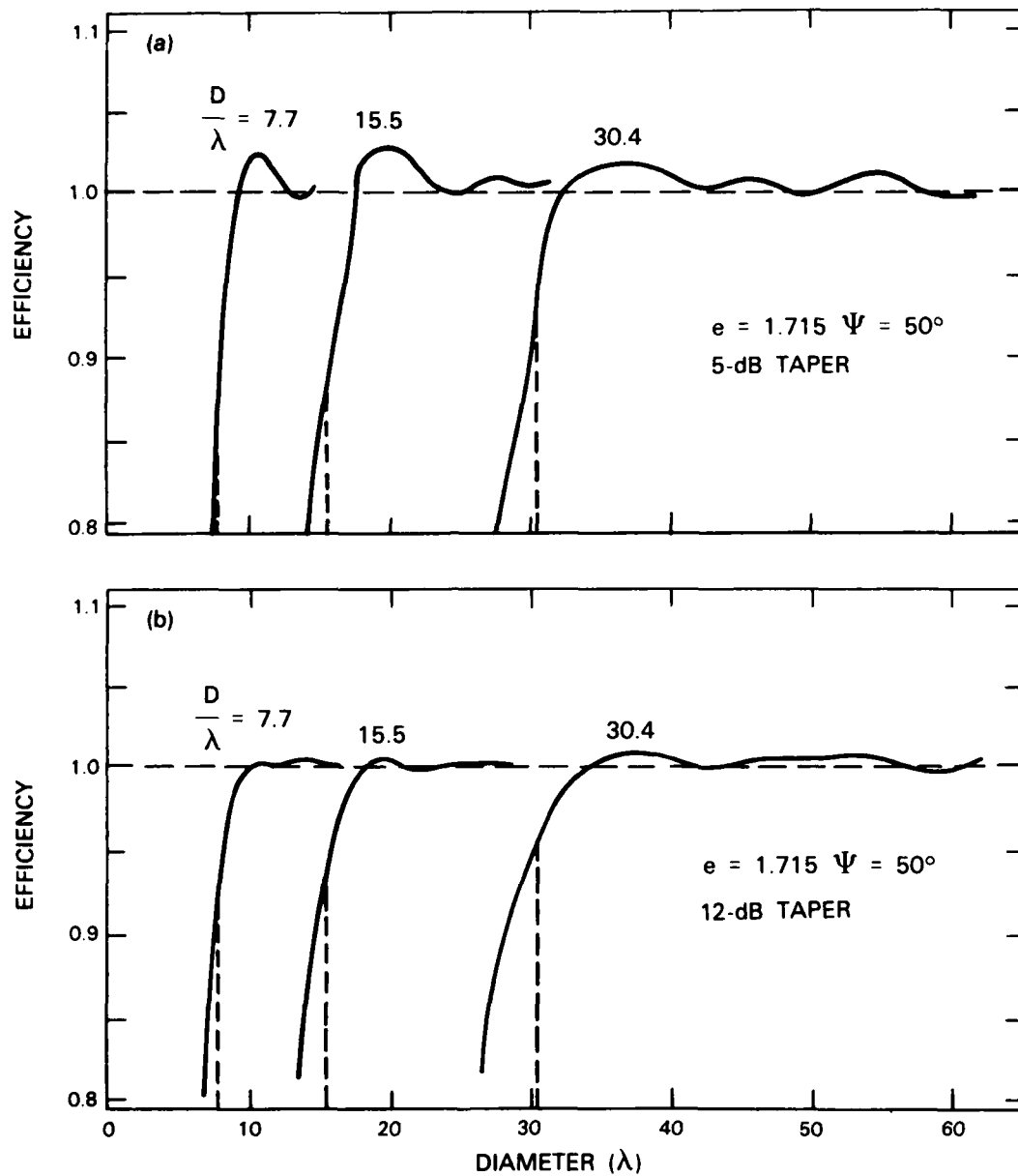
-30-

Fig. 15. Subreflector efficiency as a function of diameter, for two values of illumination taper.

the smaller subreflectors. With an illumination taper of 5 dB, the efficiency of the 7.7 λ subreflector is about 0.83, and that of the 30.4 λ subreflector is about 0.91. With an illumination taper of 12 dB the efficiency is greater, being about 0.91 and 0.95 for the 7.7 λ and the 30.4 λ subreflectors, respectively. It is also observed that making the subreflector diameter about 2 λ greater than the ray-optics diameter is sufficient to achieve unit efficiency. The lower efficiency of subreflectors truncated at the ray-optics boundary is the result of edge diffraction. As reported in the previous section, the effects of edge diffraction is a reduction of about 6 dB, and a deviation of about 30°, of the intensity and phase of the field in edge directions. Since, to a first order, these effects are independent of subreflector geometry, the results obtained for the axially symmetric, dual-reflector antenna of specific geometry, also apply to other geometries.

## 5.0   CONCLUSIONS

The scattering characteristics of offset hyperboloid reflectors with projected diameters ranging from 8.3 $\lambda$ to 35.6 $\lambda$ were studied analytically and experimentally with results in very good agreement.  The physical-optics analysis was carried out using a computer-implemented, patch simulation technique of arbitrary shaped reflectors (computer modelling), which proved to be time efficient, accurate and simple to apply.  The computer modelling technique was also used in a study to determine the minimum value of subreflector diameter required to optimize gain in dual-reflector antennas, and that value was found to be about two wavelengths greater than the ray-optics diameter.

REFERENCES

1.  A. R. Dion, "Investigations of Effects of Surface Deviations on Haystack Antenna Radiation Patterns," Technical Report 324 Lincoln Laboratory, M.I.T. (29 July 1963) DDC-418740.

2.  A. R. Dion, "Minimum Directive Gain of Hopped-Beam Antennas," Technical Note 1979-33, Lincoln Laboratory, M.I.T. (11 June 1979) DTIC-AD-A069095.

3.  S. Silver, "Microwave Antenna Theory and Design," (McGraw-Hill, New York 1949) p. 140.

4.  S. Silver, op. cit., p. 167.

5.  W. V. T. Rusch, "Scattering from a Hyperboloidal Reflector in a Cassegrainian Fed System," IEEE Trans. Antenna and Propag., AP-11, 414 (July 1963).

6.  D. C. Weikle, "Earth Coverage Corrugated Horns," Technical Report 656, Lincoln Laboratory, M.I.T. (19 July 1983) DTIC-AD-A133250.

7.  S. Silver, op. cit., p. 425.

| REPORT DOCUMENTATION PAGE | | READ INSTRUCTIONS<br>BEFORE COMPLETING FORM |
|---|---|---|
| **1. REPORT NUMBER**<br>ESD-TR-84-050 | **2. GOVT ACCESSION NO.**<br>AD-A149 224 | **3. RECIPIENT'S CATALOG NUMBER** |
| **4. TITLE** *(and Subtitle)*<br><br>Electromagnetic Scattering by Arbitrarily Shaped<br>Reflectors: Subreflector Efficiency | | **5. TYPE OF REPORT & PERIOD COVERED**<br><br>Technical Report |
| | | **6. PERFORMING ORG. REPORT NUMBER**<br>Technical Report 662 |
| **7. AUTHOR(s)**<br><br>Andre R. Dion and Letitia V. Muresan | | **8. CONTRACT OR GRANT NUMBER(s)**<br><br>F19628-85-C-0002 |
| **9. PERFORMING ORGANIZATION NAME AND ADDRESS**<br>Lincoln Laboratory, M.I.T.<br>P.O. Box 73<br>Lexington, MA 02173-0073 | | **10. PROGRAM ELEMENT, PROJECT, TASK<br>AREA & WORK UNIT NUMBERS**<br>Program Element Nos. 63431F<br>and 33601F<br>Project Nos. 2029 and 6430 |
| **11. CONTROLLING OFFICE NAME AND ADDRESS**<br>Air Force Systems Command, USAF<br>Andrews AFB<br>Washington, DC 20331 | | **12. REPORT DATE**<br>31 October 1984 |
| | | **13. NUMBER OF PAGES**<br>42 |
| **14. MONITORING AGENCY NAME & ADDRESS** *(if different from Controlling Office)*<br><br>Electronic Systems Division<br>Hanscom AFB, MA 01731 | | **15. SECURITY CLASS.** *(of this report)*<br><br>Unclassified |
| | | **15a. DECLASSIFICATION DOWNGRADING SCHEDULE** |

**16. DISTRIBUTION STATEMENT** *(of this Report)*

Approved for public release; distribution unlimited.

**17. DISTRIBUTION STATEMENT** *(of the abstract entered in Block 20, if different from Report)*

**18. SUPPLEMENTARY NOTES**

**19. KEY WORDS** *(Continue on reverse side if necessary and identify by block number)*

| | |
|---|---|
| scattering | offset cassegrain antenna |
| hyperboloid | reflector antennas |
| physical optics | |

**20. ABSTRACT** *(Continue on reverse side if necessary and identify by block number)*

A general expression for the electromagnetic scattering by an arbitrary shaped reflector is developed and applied in a computer model of offset hyperboloid reflectors. The computed scattering is shown to be in excellent agreement with scattering measurements made on an offset reflector of projected diameter = 24 cm, at frequencies of 10.35 GHz, 20.7 GHz and 44.5 GHz. Next, using the computer model, the efficiency of the subreflector in a dual-reflector antenna is calculated as a function of subreflector diameter and for two values of illumination taper. For subreflectors truncated at the ray-optics boundary the calculated efficiency is 0.83 and 0.91, respectively, for truncation diameter of 7.7 $\lambda$ and 30.4 $\lambda$, with 5 dB of illumination taper; these respective efficiencies increase to 0.91 and 0.95 with 12 dB of illumination taper. However, subreflectors of diameter about two wavelengths larger than the ray-optics diameter have very nearly unit efficiency.

**DD** **FORM 1473** EDITION OF 1 NOV 65 IS OBSOLETE
**1 Jan 73**

# END

# FILMED

2-85

# DTIC